Electroanalysis

WILEY-VCH

ELECTROANALYSIS
An International Journal Devoted to Electroanalysis, Sensors and Bioelectronic Devices

RESEARCH ARTICLE OPEN ACCESS

Detection of Diclofenac and Carbamazepine using Voltammetry and Flow Injection Analysis at Boron-Doped Diamond Thin-Film Electrodes

Aaron I. Jacobs[1] | Simphiwe Zwane[1,2] | Romana Jarošová[1] | Marissa D. Zamora[1] | Alex T. Kuvarega[2] | Greg Swain[1]

[1]Department of Chemistry, Michigan State University, East Lansing, Michigan, USA | [2]Institute for Nanotechnology and Water Sustainability, College of Science, Engineering and Technology, University of South Africa, Florida Science Campus, South Africa

Correspondence: Greg Swain (swain@chemistry.msu.edu)

Received: 22 April 2024 | **Revised:** 21 August 2024 | **Accepted:** 3 September 2024

Funding: Army Research Office (GMS), Grant/Award Number: #W911-NF-14-10063; Fulbright Scholar Program through the National Research Foundation, Grant/Award Number: 145308; Institute for Nanotechnology and Water Sustainability; University of South Africa; National Science Foundation, Grant/Award Number: CHE-2150173; National Science Foundation

Keywords: boron doped diamond | carbamazepine | diclofenac | square wave voltammetry and flow injection analysis with amperometric detection

ABSTRACT

The electrochemical detection of two pharmaceuticals, diclofenac (DCF) and carbamazepine (CBZ), was investigated as an oxidation current using boron-doped nanocrystalline diamond (BDD) thin-film electrodes. Both voltammetry and flow injection analysis with amperometric detection (FIA-EC) were used to measure the drugs in standard solutions and a urine simulant. The oxidation potential for DCF was *ca.* 0.7 V vs. Ag/AgCl (3 M KCl) in 0.1 M phosphate buffer (pH 7.2) and was *ca.* 1.2 V for CBZ in 0.1 M perchloric acid. The DCF oxidation reaction was diffusion controlled at the detection potential with evidence of some surface fouling by reaction products. The CBZ oxidation reaction was also controlled by diffusion at the detection potential, but with no surface fouling. The voltammetric peak currents for both drugs increased linearly with the concentration in the micromolar range ($r^2 \geq 0.994$). FIA-EC analysis of DCF and CBZ revealed a linear dynamic range from at least 0.1 to 100 μM with the actual minimum concentration detectable (S/N = 3) being less than the lowest concentration measured. The recovery percentage for DCF in the urine simulant ranged from 94–108% and from 97–100% for CBZ, both assessed using square wave voltammetry. FIA-EC data revealed that the BDD electrodes offer excellent intra and inter-electrode repeatability with an RSD for DCF and CBZ of 4.90% and 3.81%, respectively. The BDD electrode provided good reproducibility and response stability over eight days of continuous use detecting both DCF and CBZ. Overall, BDD electrodes are a viable material for the sensitive, selective, and reproducible electrochemical detection of these two pharmaceuticals.

1 | Introduction

The availability of therapeutic pharmaceuticals has significantly enhanced human health by curing and controlling various diseases and maladies. The production and consumption of pharmaceutical products have rapidly increased with the development of medicine. Anti-inflammatory drugs, antibiotics, and analgesics are the most common drugs used around the world. Consequently, the emergence of water-soluble and pharmacologically-active organic micropollutants or pharmaceutical-active compounds (PhACs) has gained much attention worldwide [1–4]. Humans use many pharma-

ceuticals for their health in everyday life. Large quantities of these drugs are also used in veterinary medicine for animal health care to prevent and treat disease and to increase economic value of commercial livestock [1–6]. After ingestion, pharmaceuticals are excreted in urine and feces as active substances and or metabolites [5, 6]. Besides human and animal sources, pharmaceuticals enter the environment as effluent from the pharmaceutical industry. In many cases, these drugs and metabolites are not effectively removed by conventional water treatment processes, therefore, they end up as constituents in drinking water [7, 8]. The presence of these active drugs and metabolites in water sources presents a pollution problem for society and is an ongoing health issue for human and aquatic life.

Pharmaceuticals that reach both surface water and groundwater bodies originate from several sources as indicated above. Pharmaceuticals found in high concentrations in wastewater include non-steroidal anti-inflammatory drugs (NSAIDs), β-blockers and psychoactive compounds, analgesics, antibiotics, endocrine disruptors, antiretroviral drugs, and drugs to treat cancer [9, 10]. As mentioned above, the main concern is that conventional water treatment processes can be ineffective at removing these chemical contaminants. Improved technologies are needed for their elimination. Furthermore, new analytical methods for identifying and quantifying these compounds are increasingly being developed [11–13].

Electrochemical techniques are useful for detecting electroactive pharmaceuticals and metabolites as the methods are inexpensive, field deployable, require minimal training and expertise to operate, and provide, in many cases, low detection limits, excellent sensitivity and superb reproducibility. In this work, we report on the electrochemical detection of two pharmaceuticals, diclofenac (DCF) and carbamazepine (CPZ), as oxidation currents using boron-doped nanocrystalline diamond (BDD) electrodes. The molecular structures of the two drugs are presented below. BDD electrodes offer well known properties for electroanalysis including (i) low and stable background current leading to enhanced signal-to-background ratios, (ii) a wide working potential range, (iii) microstructural stability at extreme potentials, and (iv) reproducible and stable oxidation and reduction currents for redox-active compounds.

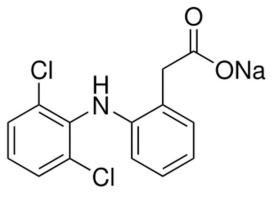

Diclofenac sodium salt (DCF)

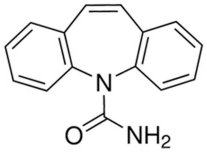

Carbamazepine (CBZ)

Diclofenac (DCF) is a commonly used synthetic non-steroidal drug (NSAID) because of its analgesic, anti-inflammatory, and antipyretic properties [14]. Carbamazepine (CBZ) is used as mood stabilizing drug and to treat bipolar effective disorder like resistant schizophrenia, ethanol withdrawal, restless leg syndrome, psychotic behavior associated with dementia and post-traumatic stress disorders [15–17]. Generally speaking, whenever an individual consumes these drugs, about 2–3% of the unmetabolized drug is excreted through urine and enters aquatic environments [7, 8].

DCF and CBZ are considered emerging chemical contaminants in ground and surface waters and can cause adverse effects in the ecosystem due to continuous exposure and the synergistic effects of their mixtures [18–21]. The major channels for these compounds to enter water bodies include but are not limited to large consumption where some molecules are excreted in urine, inappropriate disposal, and poor biodegradation by conventional wastewater or water treatment plants. The quantification of trace quantities of these drugs in environmental waters allows for proper evaluation of human exposure and ramifications of exposure.

Both DCF and CBZ are electrochemically active and undergo irreversible electrooxidation. Others have investigated the electrooxidation reaction mechanism of these two drugs. DCF loses two electrons and two protons whereas CBZ loses four electrons and two protons [22–31].This was determined by the pH dependence of the DCF and CBZ oxidation potentials and scan rate analysis of the electrooxidation process. Dimers are created when DCF and CBZ undergo electrochemical oxidation. A cation radical is initially formed when DCF loses one electron. Two DCF radicals then combine to form a bridge between phenyl ring carbons, resulting in a dimer. Likewise, the electrooxidation of CBZ initiates with removal one electron from the nitrogen atom generating a CBZ cation radical. The cation radical interacts with a second radical forming a dimer. The proposed oxidation reaction mechanisms reported for DCF and CBZ are presented in Figure 1 [22–31].

DCF has previously been detected at unmodified BDD electrodes using various electroanalytical techniques, including differential pulse voltammetry (DPV) [32], square wave voltammetry (SWV) [22], and flow injection analysis (FIA) with amperometric detection [33]. The DCF oxidation potential occurs between *ca.* 0.7 and 1.0 V vs. Ag/AgCl, depending on the electrolyte pH used. In all cases, the peak current increased linearly with the DCF concentration in the ranges reported with excellent sensitivity and low detection limits ($\leq$0.15 μM). To our knowledge, CBZ has not been analytically detected at unmodified BDD electrodes. However, numerous studies have examined BDD anode utility for eliminating CBZ from municipal water and wastewater [29, 34].

FIA is a promising technique for the rapid and sensitive analysis of CBZ and DCF in aqueous solution. The technique is based on the injection of a small sample into a carrier solution for transport to a detector. Reagents can also be mixed with the analyte sample prior to reaching the detector to enhance detection or render an undetectable analyte detectable [35]. Electrochemical detection is commonly coupled with FIA. BDD electrodes are an excellent choice for FIA with electrochemical detection (FIA-EC) due to their superlative properties over other carbon electrodes [36]. As an example, BDD thin-film electrodes have been used with FIA-EC to detect pyocyanin in 0.1 mol L^{-1} phosphate buffer (pH 7.4) [37]. In another example, researchers simultaneously detected acetami-

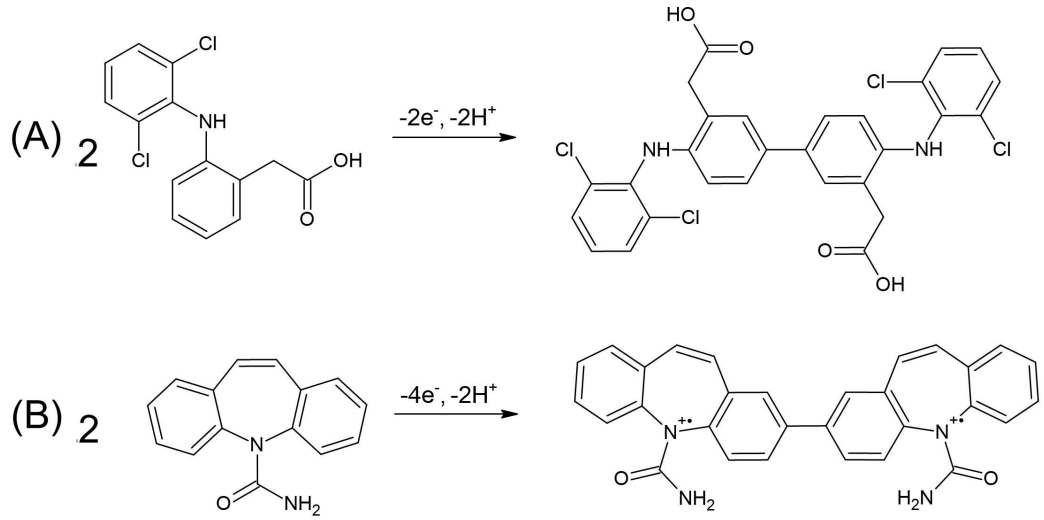

FIGURE 1 | The proposed electrochemical oxidation reaction mechanisms for (A) DCF [22–27] and (B) CBZ [28–31]. Structures drawn with ChemSketch.

nophen and tramadol using FIA-EC with multiple pulse amperometric detection using a cathodically pretreated BDD electrode [38]. The investigation focused on optimizing the potential, performing measurements at different concentrations, and assessing response reproducibility. FIA has gained interest due to the low cost of the equipment, high sample throughput, reduced consumption of reagents and reduced waste generation.

Herein, we report on the oxidative detection of DCF and CBZ in standard aqueous solutions and a spiked urine simulant using cyclic and square wave voltammetry and FIA-EC. The working electrode was boron-doped nanocrystalline diamond (BDD) [36, 39–41]. The results revealed that BDD thin-film electrodes provide sensitive, stable, and reproducible detection of DCF at *ca.* 0.7 V and CBZ at *ca.* 1.2 V vs. Ag/AgCl.

2 | Experimental Section

2.1 | Chemicals and Reagents

All chemicals were purchased from Sigma-Aldrich as analytical grade quality, or better. These include sodium phosphate monobasic dihydrate ($\geq$99%); sodium phosphate dibasic dihydrate ($\geq$99%); diclofenac sodium salt (DCF, 98%); carbamazepine (CBZ, $\geq$99%); potassium hexacyanoferrate ($K_3Fe(CN)_6$, $\geq$99%); potassium chloride (KCl, $\geq$99%); isopropanol (IPA, $\geq$99.5%); methanol ($\geq$99.9%); perchloric acid ($HClO_4$, 70% w/w); hydrochloric acid (HCl, $\geq$37% w/w); and sodium hydroxide (NaOH, $\geq$97.0%). The urine simulant was Sigmatrix Urine Diluent, also from Sigma-Aldrich. This is a non-biological diluent that mimics human urine. The simulant, as specified by the supplier, is a buffered solution (pH 6.5–7.2) containing calcium chloride, magnesium chloride, potassium chloride, sodium chloride, sodium phosphate, sodium sulfate, urea, and creatinine with sodium azide as a preservative. IPA,distilled and stored over activated carbon, was used for BDD electrode cleaning prior to use.

2.2 | Solutions

Initially, the pharmaceutical powders were dissolved in methanol to prepare 10 mM stock solutions. Then, DCF and CBZ stock solutions were diluted in 0.1 M phosphate buffer (PB, pH 7.2) and 0.1 M perchloric acid ($HClO_4$), respectively. The final working solution contained 1% methanol (v/v). All subsequent dilutions contained the same methanol volume fraction. All solutions were prepared using ultrapure water ($\geq$ 18 MΩ-cm) supplied by a Millipore-Q water purification system (Billerica, USA). Urine diluents were used as received. For voltammetric analysis, urine simulants were diluted to 10 mL with 0.1 M PB (for DCF) or 0.1 M $HClO_4$ (for CBZ) at a 1:1 (v/v) ratio using a 5 mL volumetric pipette. The urine simulant mixtures contained of drug concentrations of 10, 25 and 50 μM.

2.3 | Boron-Doped Diamond Thin-Film Deposition

The nanocrystalline diamond thin-film (BDD) electrodes were deposited by microwave-assisted chemical vapor deposition. Deposition was performed on highly boron-doped Si (111) substrates (0.05 cm thick by 1 cm^2 in area, ~10^{-3} Ω-cm, Virginia Semiconductor Inc., Fredricksburg, VA) using a 1.5 kW reactor (Seki Diamond Systems, Japan). All source gases, methane (CH_4), hydrogen (H_2) and diborane diluted in hydrogen (0.1% (v/v) B_2H_6 in H_2), were ultrahigh purity grade (99.999%). Prior to growth, the Si substrate was ultrasonically cleaned in acetone for 15 min, abraded in a diamond powder (100 nm diam.)/ultrapure water slurry paste for 3 min on a felt pad, rinsed with ultrapure water, and then ultrasonically seeded with nanodiamond particles (Opal Seed suspension, Adamas Nanotechnologies Inc., Raleigh, NC). Opal seed consists of 30 nm nanodiamond powder particles (nominally) suspended in dimethyl sulfoxide (DMSO). After ultrasonic seeding for 30 min in a glass beaker, the substrate was rinsed with ultrapure water, and then dried with N_2 gas before placement in the CVD reactor chamber. The scratches introduced by the diamond powder, residual diamond powder

embedded from the abrading, and embedded diamond power particles from the ultrasonic seeding all serve as initial nucleation sites for diamond film growth.

For the BDD thin-film growth, a 1% (v/v) CH_4/H_2 source gas mixture was employed with 10 ppm of diborane (B_2H_6) added for boron doping. The total gas flow rate was 200 sccm with 2.00 sccm CH_4, 2.00 sccm B_2H_6/H_2, and 196 sccm H_2. The microwave power was 1000 W, and the system pressure was 35 torr. The substrate temperature during the deposition was approximately 825°C, as estimated with a disappearing-filament optical pyrometer. These deposition conditions produced a 2–4 μm thick BDD film during a growth time of 4–6 h. The boron doping level was in the low 10^{21} cm^{-3} range, based on Raman spectroscopic and other electrical measurement data for diamond films prepared using similar growth conditions [36, 39, 40]. The film's electrical resistivity was $\leq$0.01 ohm-cm. At the end of the deposition, the CH_4 and B_2H_6 flows were stopped while the H_2 flow continued with the plasma still ignited. The specimen was then cooled in the presence of atomic hydrogen in the H_2 plasma by slowly lowering the microwave power and system pressure over a 30-min period to decrease the estimated substrate temperature to below 400°C. This post-growth cooling is essential for maintaining a hydrogen surface termination and minimizing surface reconstruction to a sp^2-bonded carbon phase that would be caused by surface hydrogen desorption at the higher growth temperature in the absence of atomic hydrogen.

The material and electrochemical properties of the BDD thin-film electrodes were characterized using scanning electron microscopy (SEM), Raman spectroscopy, and varied scan rate cyclic voltammetry. These characterization data are presented in Figure S1. The SEM micrographs reveal the BDD thin-film electrodes are polycrystalline with the individual crystallites that are hundreds of nanometers in dimension. The Raman spectrum is characteristic of a heavily boron-doped diamond film with intense peaks at 480 and 1220 cm^{-1} and a weakly intense peak at 1545 cm^{-1}. The latter results from scattering by small amounts of non-diamond sp^2 carbon impurity. The zone-center optical phonon of diamond is also observed, but is downshifted from the expected 1332 cm^{-1} position to 1305 cm^{-1}. Varied scan rate cyclic voltammetric analysis was performed using 5 mM $K_3Fe(CN)_6$ dissolved in 1 M KCl as the soluble redox test system. Both the oxidation and reduction peak currents varied linearly with scan $rate^{1/2}$ reflective of reaction rates limited by semi-infinite linear diffusion of the analyte to the electrode surface. The ΔE_p was 0.163 ± 0.028 V (mean $\pm$ std. dev. for $n = 3$ BDD electrodes, 0.05 $V s^{-1}$). This trend is consistent with quasi-reversible electron-transfer kinetics at the BDD electrodes. The i-E curves were not corrected for any iR effects. The electron transfer kinetics for this redox system are affected by the electronic properties of the electrode, the surface cleanliness and the surface carbon-oxygen functional group coverage–with slower kinetics for electrodes with increasing carbon-oxygen functional group coverage [42]. The large ΔE_p is attributed to the presence of surface carbon-oxygen functional groups on these "used" BDD electrodes. Overall, these characterization data are consistent with previous reports for similar BDD electrodes [36, 39, 40].

2.4 | Analytical Procedure for Voltammetric Detection

The electrochemical measurements were performed using a commercial workstation (CH Instruments, Model 832 A, Ausin TX) and a single compartment glass cell [36]. A conventional three-electrode configuration was used with a BDD working electrode, a commercial Ag/AgCl reference electrode (3 M KCl), and a platinum wire counter electrode. The reference electrode was periodically calibrated against an SCE reference electrode. The Ag/AgCl reference electrode had a potential of about −36 mV vs. SCE. The BDD thin-film electrode was mounted at the bottom of the glass cell using a Viton O-ring to define the area of the electrode exposed to the electrolyte solution (0.32 cm^2). Electrical contact was made on the backside of the Si substrate by gently abrading the surface, wiping the debris away with an IPA-wetted cotton swab, and then coating the area with a layer of graphite from a pencil. A copper foil current collector was then placed in physical contact with the backside of the Si substrate. All measurements were performed at room temperature between 20–23°C. Once mounted in the cell, the BDD electrode surface received a final cleaning by soaking in ultrapure lPA for 20 min followed by rinsing with ultrapure water [36, 43].

Cyclic voltammetry (CV) was used to evaluate the oxidation response of the two pharmaceuticals as a function of the scan rate. Between each DCF voltammetric measurement, the electrode surface was soaked with IPA for 5 min in the cell followed by an ultrapure water rinse to remove adsorbed oxidized species that caused some electrode fouling. Then, the DCF solution was replaced, and a subsequent measurement was made. Between each CBZ voltammetric measurement, the solution was mixed with a Pasteur pipette to eliminate the depletion layer formed at the electrode surface. The electro-oxidation of CBZ and DCF was also studied using square wave voltammetry (SWV) at concentrations from 0.1 to 100 μM. The SWV parameters were as follows: increment = 2 mV, amplitude = 25 mV, and frequency = 15 Hz. A calibration curve was constructed from the peak current response as a function of the pharmaceutical concentration . The response curves were recorded from low concentration to high. Between each SWV measurement of DCF, the electrode in the cell was contacted with ultrapure IPA and rinsed with water, as described above. Between each SWV recording of CBZ, the electrode in the cell was only rinsed with water. The detection of CBZ and DCF was also performed using SWV in spiked urine simulant samples prepared with urine diluent, as described above. The simulant was stored at ~3°C when not in use. The detected concentration of each drug was determined by the standard addition method from which the percent recovery was calculated.

2.5 | Analytical Procedure for Flow Injection Analysis

The flow injection analysis system consisted of an Alltech HPLC pump (Model 3012, Grace) and a six-port injection valve (Model 7125, Rheodyne) with a 20 μL injection loop connected to the thin-layer, crossflow electrochemical cell. The flow cell design is diagrammed in Figure S2 [44, 45]. It consists of a two-piece Kel-f body with the top piece having the entrance and

exit ports for the carrier solution and a port for a no-leak mini-Ag/AgCl reference electrode (3 M KCl, eDAQ, Model ET073). A stainless tube on the exit port served as the counter electrode. The working electrode was placed between the bottom and top piece of the cell with a gasket in between. The area of the working electrode was defined by a rectangular flow channel (ca. 1.05×0.1×0.01 cm) cut into the polyimide (Kapton) gasket material. Electrical contact was made using a thin copper foil placed against the back side of the BDD electrode (conducting Si substrate scratched, cleaned and coated with graphite). The cell volume was ca. 1 μL assuming no compression of the gasket when the cell is tightened. The working electrode surface was cleaned while mounted in the flow cell by flowing through a small volume of ultrapure IPA.

Potentials were controlled and currents measured using a commercial electrochemical workstation (CH Instruments, Model 832 A) operated in the amperometric detection mode. The analyte solution was injected (20 μL) 600 s after a potential was applied, which was sufficient time for the background current to stabilize. Three repeat injections of each analyte solution were used to assess response reproducibility when generating a calibration curve. The carrier solution was 0.1 M PB (pH 7.2) for DCF and 0.1 M $HClO_4$ for CBZ. The limit of detection was determined experimentally at a signal-to-noise ratio of 3 and calculated theoretically using the equation $3\,s/m$ where s is the standard deviation of the mean background signal at the detection potential and m is the slope of calibration curve for the drug.

3 | Results

3.1 | Cyclic Voltammetric Behavior of DCF and CBZ

The CV response of both drugs was investigated as a function of cycle number. Figure 2A shows the curves for 100 μM DCF in 0.1 M PB (pH 7.2) at 0.05 V s^{-1} over 10 cycles. An irreversible oxidation peak is seen at 0.7 V followed by a second irreversible oxidation peak at 1.05 V. The peak currents at these two potentials decreased with increasing cycle number. This is primarily attributed to a depletion layer effect as there is no corresponding reduction current on the reverse scan within the scan range probed to regenerate the reactant in the interfacial region. After mixing the DCF solution with a Pasteur pipette, the peak current was restored to about 80% of its original magnitude. Therefore, depletion layer formation contributed to most but not all the current decrease with increasing cycle number. During the reverse sweep of the initial scan, a reduction peak emerges at *ca.* 0.25 V. This reduced species is then re-oxidized on the reverse sweep of the next cycle at *ca.* 0.4 V. This reversible peak current is largest on the first cycle, but then decreases with cycle number. Since the reversible peak only appeared after the initial DCF oxidation at 0.7 V, it is due to the formation of an electroactive DCF oxidation intermediate or product. The origin of the reversible species and its influence on electrode fouling is further explored in the *Discussion* section below.

Figure 2B shows the curves for 100 μM CBZ in 0.1 M $HClO_4$ at 0.05 V s^{-1} for 10 cycles. The CBZ oxidation reaction is chemically irreversible as there is no reduction peak observed on the reverse sweep within the potential window probed, even when the window was extended down to 0 V (not shown). The CBZ current also decreased with successive cycles. After mixing with a Pasteur pipette, the current was fully restored. Therefore, the current diminution was caused only by a depletion layer effect. Notably, the peak currents for CBZ are ~2 times larger than the currents for DCF at the same solution concentration. This is expected as the CBZ oxidation involves four electrons transferred whereas the DCF only involves two electrons transferred per molecule.

Figure 3A shows cyclic voltammetric *i-E* curves for 100 μM DCF in 0.1 M PB (pH 7.2) at different scan rates from 0.05 to

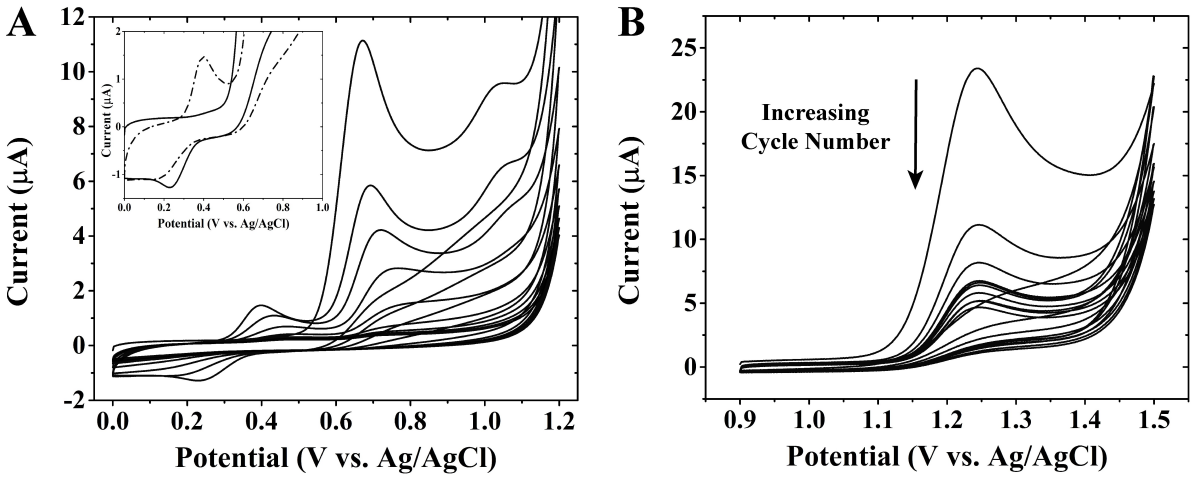

FIGURE 2 | Cyclic voltammetric *i-E* curves for (A) 100 μM DCF in 0.1 M PB (pH 7.2) and (B) 100 μM CBZ in 0.1 M $HClO_4$ at a BDD thin-film electrode. Curves are presented for ten cycles at 0.05 V s^{-1}. Inset shows the first (solid) and second (dashed) cycles. In both figures, the voltammetric currents are decreasing with cycle number. The initial forward scans for the two drugs were begun at 0 and 0.9 V, respectively, both in the positive-going direction.

0.40 $V s^{-1}$. The first scan at each scan rate is presented since it showed the largest current and was not affected by depletion layer formation or surface fouling. A well-defined oxidation peak is seen at 0.68 V for the 0.05 $V s^{-1}$ scan. The peak current increases and the peak potential shifts positively with increasing scan rate. The inset shows a plot of the oxidation peak current versus the square root of the scan rate. The trendline is linear with a correlation coefficient of 0.9999. The corresponding regression equation is shown below. The values are presented as the mean ± std. dev. for three different BDD thin-film electrodes.

$$i_p = 1.47\ (\pm 0.02) \times 10^{-6}\ v^{1/2}\ + 0.80(\pm 0.36) \times 10^{-6}$$

The linear relationship observed between the peak current and the square root of the scan rate indicates the DCF oxidation reaction occurs through diffusion-controlled transport to the BDD electrode at these potentials. The positive shift of the oxidation peak potential with scan rate is consistent with sluggish electron transfer (quasi-reversible) kinetics at the BDD electrode.

Figure 3B shows cyclic voltammetric *i-E* curves for 100 μM CBZ in 0.1 M $HClO_4$ at different scan rates from 0.05 to 0.40 $V s^{-1}$. The first scan at each scan rate is presented. A well-defined oxidation peak is seen at 1.23 V for the 0.05 $V s^{-1}$ scan. The peak current increases and the peak potential shifts positively with increasing scan rate. The inset shows a plot of the oxidation peak current versus the square root of scan rate. The trendline is linear with a correlation coefficient of 0.9999. The corresponding regression equation is shown below. The values are presented as the mean ± std. dev. for three BDD electrodes.

$$i_p = 2.27\ (\pm 0.01) \times 10^{-6}\ v^{1/2}\ + 7.7\ (\pm 0.2) \times 10^{-6}$$

The linear relationship between the peak current and the square root of scan rate indicates the CBZ oxidation reaction proceeds through diffusion-controlled transport to the BDD electrode at these potentials.

3.2 | Square Wave Voltammetric Analysis of DCF and CBZ

SWV was used to study the concentration dependence of the oxidation peak currents for each drug. Figure 4A shows curves recorded for different concentrations of DCF in 0.1 M PB (pH 7.2) at a BDD electrode. Curves are presented for concentrations from 0.1 to 100 μM. The DCF oxidation peak potential is observed at 0.65 V. The voltammogram for the electrode in PB electrolyte only is also presented (dashed black curve) for comparison. There is no oxidation current in the potential region around 0.65 V. This confirms the oxidation current seen at this potential is attributable to the drug. The peak current increases with increasing drug concentration. The peak current for the 0.1 μM concentration (solid red curve) is above a signal-to-noise (S/N) of 3 so the minimum concentration detectable is actually lower than this value. The figure inset shows a plot of the oxidation peak current versus the DCF concentration from 0.1 to 100 μM (4 order of magnitude linear dynamic range). The trendline is linear with a correlation coefficient of 0.992. The response reproducibility for the BDD electrodes is quite good based on the small error bars seen at each concentration. The slope of the response curve for three electrodes is nominally 57 (± 2) μA mM^{-1}. This sensitivity is comparable to SWV analysis of DCF at BDD electrodes reported by other authors [22, 32].

Figure 4B shows the SWV *i-E* curves recorded for 0.1 to 100 μM CBZ concentrations in 0.1 M $HClO_4$ at a BDD thin-film electrode. The oxidation peak potential is seen at 1.2 V. The curve for just the $HClO_4$ is also presented (dashed black curve) and no oxidation current is seen in the potential region around 1.2 V. This confirms the oxidation current seen at this potential is attributable to the drug. The peak current for CBZ oxidation increases with increasing analyte concentration. The peak current for the 0.1 μM concentration (solid red curve) is above a signal-to-noise (S/N) of 3 so the minimum concentration detectable is also below this value. The inset shows a plot of the oxidation peak current versus the CBZ concentration. A

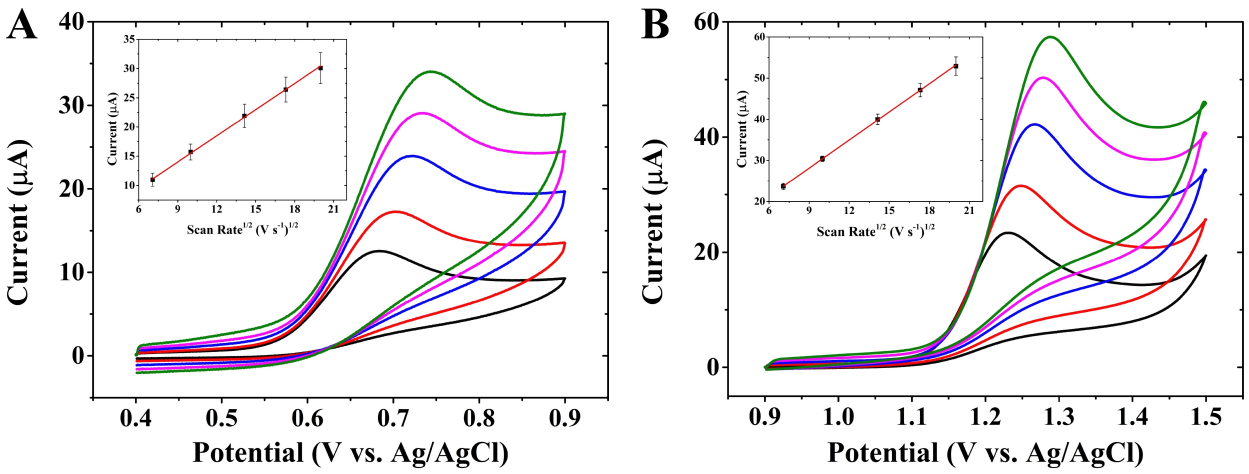

FIGURE 3 | Cyclic voltammetric *i-E* curves for (A) 100 μM DCF in 0.1 M PB (pH 7.2) and (B) 100 μM CBZ in 0.1 M $HClO_4$ at a BDD thin-film electrode. Curves are presented for different scan rates up to 0.4 $V s^{-1}$. The inset presents a plot of the oxidation peak current versus the square root of scan rate. Data are presented as mean ± std. dev. for n = 3 BDD electrodes. The initial forward scans for the two drugs were begun at 0.4 and 0.9 V, respectively, both in the positive-going direction.

linear response is seen with a correlation coefficient of 0.997. The slope of the response curve for three electrodes is nominally 162 (± 5) μA mM^{-1}; about 3x larger than for DCF.

Square Wave Voltammetric Analysis of DCF and CBZ in Urine Simulant. SWV was used to investigate the oxidation current for different DCF and CBZ concentrations in the urine simulant. Figures 5A and B show voltammetric curves for selected concentrations (10, 25 and 50 μM) of DCF and CBZ, respectively. The oxidation peak potentials for the two analytes in the urine simulant are similar to the potentials in standard solutions of PB (pH 7.2) and 0.1 M $HClO_4$, as seen in Figure 4. As expected, the oxidation peak currents increase with drug concentration. Interestingly, the background current (black line) at 1.2 V in Figure 5B for the urine simulant: $HClO_4$ solution is larger than the current in just $HClO_4$ as presented in Figure 4B. The urine simulant:$HClO_4$ mixture is pH 1.4, compared to pH 1 for the $HClO_4$ alone. This small pH difference would cause only minimal change in the oxygen evolution and CBZ oxidation potentials and does not explain the increase in background current. The urine simulant contains other species that can be oxidized on BDD electrodes around these potentials, like chloride [46], urea [47], and creatinine [48]. Therefore, oxidation of these compounds is likely responsible for the increased background current at 1.2 V.

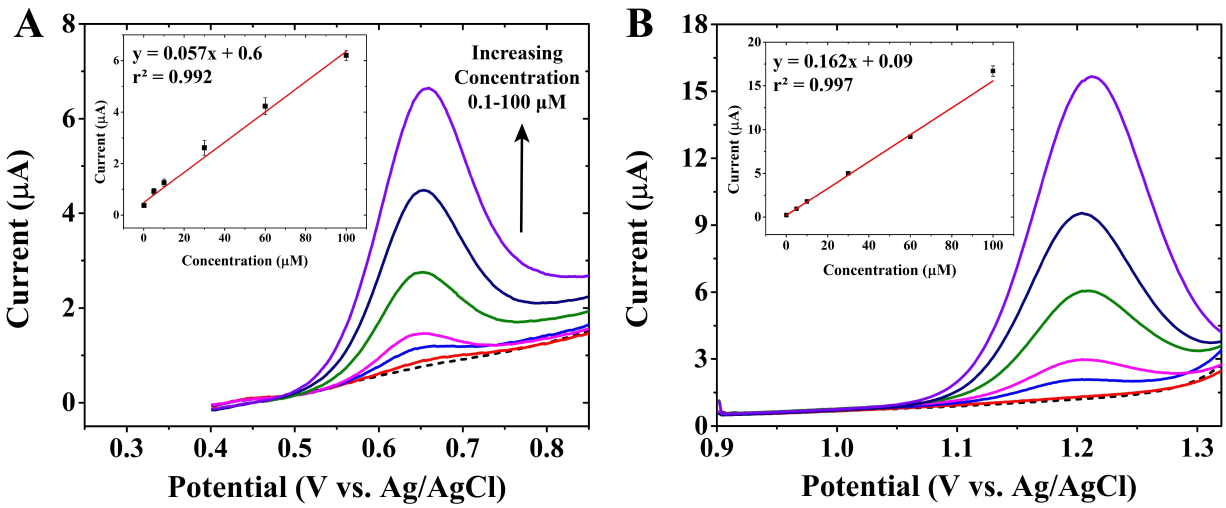

FIGURE 4 | Square wave voltammetric *i-E* curves for (A) DCF in 0.1 M PB (pH 7.2) and (B) CBZ in 0.1 M $HClO_4$ at a BDD thin-film electrode. Curves are presented for different concentrations from 0.1 to 100 μM. The inset presents a plot of the oxidation peak current versus the concentration. The dashed line represents the SWV of background electrolyte. Data are presented as mean ± std. dev. for n = 3 different BDD electrodes. The initial forward scans for the two drugs were begun at 0.4 and 0.9 V, respectively, both in the positive-going direction. SWV parameters: increment = 2 mV, amplitude = 25 mV, and frequency = 15 Hz.

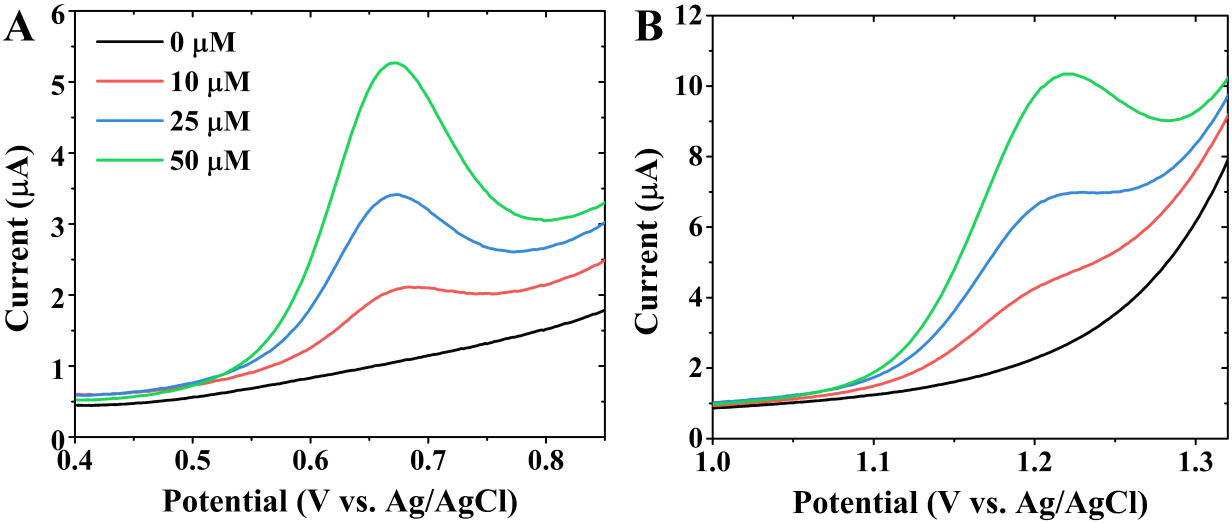

FIGURE 5 | Square wave voltammetric *i-E* curves for (A) DCF and (B) CBZ in urine simulant at a BDD thin-film electrode. Curves are presented for concentrations of 10, 25, and 50 μM. The urine simulant was prepared by a 1:1 dilution of the stock diluent with 0.1 M PB (pH 7.2) or 0.1 M $HClO_4$ for DCF and CBZ, respectively. The initial forward scans for the two drugs were begun at 0.4 and 1.0 V, respectively, both in the positive-going direction. SWV parameters: increment = 2 mV, amplitude = 25 mV, and frequency = 15 Hz.

Table 1 presents the calculated percent recoveries for a 10 μM spike of the two drugs in the urine simulant. Data is pooled for three BDD electrodes. The percent recovery was calculated by measuring the square wave voltammetric peak current, determining the concentration that current corresponds to from the analyte response curve generated by the standard addition method, and then dividing by the true spiked concentration (see the analytical expression below). The recovery percentage for 10 μM DCF was 95% with an interelectrode reproducibility of 4.8% RSD. The recovery percentage for 10 μM CBZ was also near complete at 100% with a less reproducible response of 13.3% RSD. Similar near-full recoveries have also been reported for the electrooxidation of other drugs, such as propranolol and hydrochlorothiazide, at BDD electrodes [49]. The results herein indicate the urine simulant has a more significant effect on the CBZ than on the DCF reproducibility. This is attributed to the increased background current at the CBZ detection potential arising from electroactive interferents present in the urine simulant matrix.

The electrolyte solutions were a 1:1 dilution of the urine simulant in either 0.1 M PB (pH 7.2) for DCF, or 0.1 M $HClO_4$ for CBZ. SWV parameters: increment = 4 mV, amplitude = 3 mV, and frequency = 10 Hz. The recovery values were determined by dividing the mean value of calculated drug concentration by the true concentration and multiplying by 100.

$$\%\ Recovery = \frac{[Calcuated\ Analyte\ Concentration]}{[True\ Added\ Concentration]}\ x\ 100$$

Notably, the DCF and CBZ peak currents in Table 1 are lower than the peak currents for the same concentration of spiked urine simulant shown in Figure 5. There are two reasons for this. First, the SWV pulse amplitude used for the data in the table was lower than the value used in Figures 4 and 5. This led to a two-fold decrease in current for both DCF and CBZ. Second, the current data reported in Table 1 were obtained without any cleaning of the electrode surface between the calibration and percent recovery measurements. This led to some electrode fouling from DCF oxidation products, as evidenced by the surface adsorbed species producing a reversible peak at 0.3 V in Figure 2A. With fouling, the electrochemically active surface area is reduced which decreases the oxidation peak current. Given the high percent recovery and reproducible inter-electrode responses in Table 1, the adsorbed DCF product surface coverage appears to reach a steady state without totally blocking the surface. In contrast, CBZ oxidation products did not show any adsorptive behavior.

3.3 | Electrode Response Reproducibility

The BDD electrode response reproducibility was assessed using the same SWV parameters as in the percent recovery experiments. Figure 6A and B present plots of the SWV peak current at a BDD thin-film electrode for DCF in 0.1 M PB (pH 7.2) and CBZ in 0.1 M $HClO_4$. Data are presented for two concentrations, 10 and 25 μM, over 10 measurement cycles. The same BDD electrode was used in all these measurements over the course of a single day, so these data reflect the short-term response reproducibility for a single electrode. The relative standard deviation of oxidation peak current for DCF was 2.66 and 3.12%, respectively, for the 10 and 25 μM concentrations. The relative standard deviation of the oxidation peak current for CBZ was 1.48 and 1.72%, respectively, for the 10 and 25 μM concentrations. This high level of response reproducibility is typical for all BDD electrodes used in this work and is a common characteristic of these electrodes. The data reveal good response reproducibility for both drugs at the BDD electrode.

The interday response reproducibility of BDD electrodes was also evaluated for both drugs. The SWV oxidation peak current over eight consecutive days for DCF in 0.1 M PB (pH 7.2) is presented in Figure 6C. Similar measurements for CBZ in 0.1 M $HClO_4$ are presented in Figure 6D. Data are shown for a single BDD electrode at a 10 μM analyte concentration for both drugs. Excellent response stability is seen for both. The relative standard deviation of the response for DCF was 2.39% and for CBZ was 2.01%. Overall, the BDD electrode provides good interday response reproducibility and stability for both drugs in these two carrier solutions.

3.4 | Flow Injection Analysis of DCF and CBZ with Amperometric Detection

BDD thin-film electrodes have gained popularity for electrochemical detection because of their low background current, wide working potential window, and rapid stabilization at the detection potential in FIA-EC [50]. Since DCF is oxidized at *ca.* 0.7 V in this electrolyte, the potential range between 0.4 to 1.0 V was probed to generate hydrodynamic voltammograms. CBZ is oxidized at *ca.* 1.2 V, so the potential range was set from 1.0 to 1.4 V. Figure 7 shows hydrodynamic voltammograms for (A) 100 μM DCF in 0.1 M PB (pH 7.2) and (B) 100 μM CBZ in 0.1 M $HClO_4$ for a BDD thin-film electrode. A steady-state current maximum was achieved at 0.90 V for DCF and 1.35 V for CBZ. Therefore, 1.0 V and 1.4 V were chosen as detection potentials for the two drugs, respectively.

TABLE 1 | Square wave voltammetric oxidation peak currents for 10 μM CBZ and DCF spiked into a urine simulant using three different BDD thin-film electrodes.

Pollutant	BDD 1 (μA)	BDD 2 (μA)	BDD 3 (μA)	Mean ± st. dev. (μA)	Calculated (μM)	Recovery (%)
DCF	0.0642	0.0651	0.0590	0.0628 ± 0.003	9.5 ± 0.5	95
CBZ	1.055	1.376	1.208	1.213 ± 0.161	10.1 + 1.3	100

Figure 8A presents replicate injections of DCF in the FIA-EC mode at different concentrations from 100 down to 0.1 μM. The carrier solution was 0.1 M PB (pH 7.2). Three injections of each concentration were made to assess the response reproducibility. Reproducible current responses are seen for each concentration injected with the peak height decreasing proportionally with decreasing injected analyte concentration. Figure 8A inset shows the calibration curve of peak current versus injected concentration for DCF. The response sensitivity was 4.2 (±0.2) μA mM^{-1} with good linearity across the concentration range ($r^2 = 0.994$).

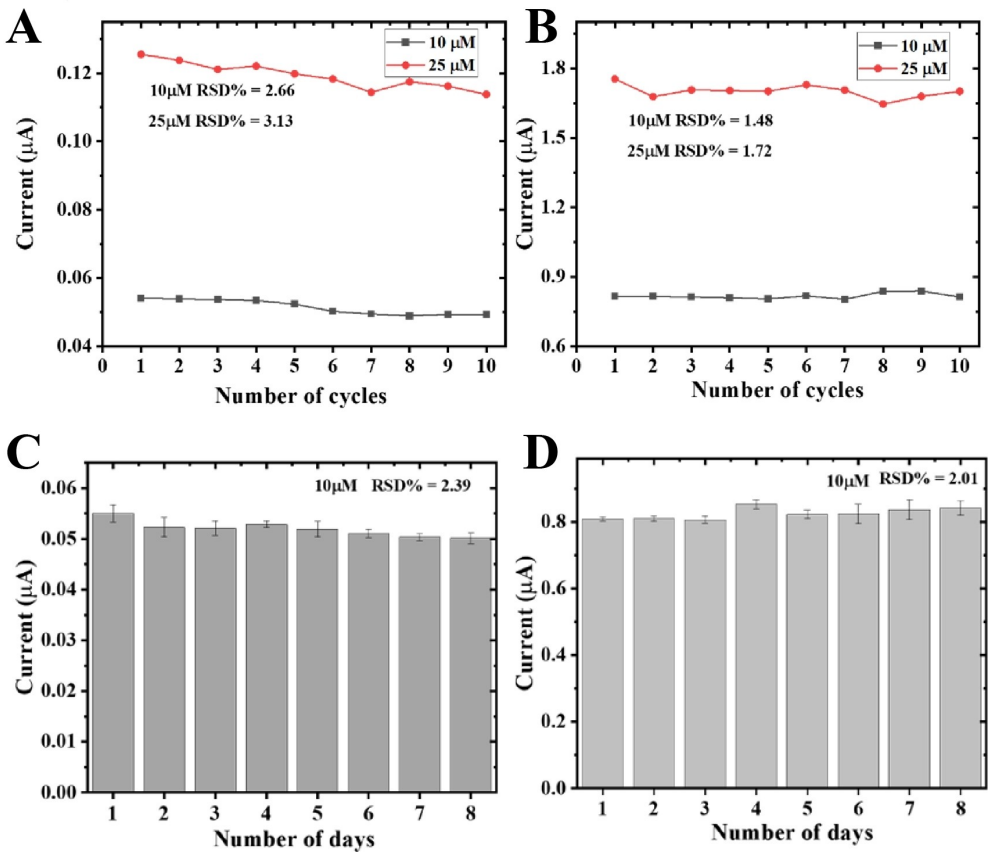

FIGURE 6 | Plots of the square wave voltammetric oxidation peak current for (A) DCF in 0.1 M PB (pH 7.2) and (B) CBZ in 0.1 M $HClO_4$ over 10 measurement cycles at 10 and 25 μM analyte concentrations. Interday SWV response reproducibility of (C) 10 μM DCF in 0.1 M PB (pH 7.2) and (D) 10 μM CBZ in 0.1 M $HClO_4$ over eight consecutive days are also presented. Data are presented for a single BDD electrode. The peak currents for DCF were measured at 0.7 V and for CBZ at 1.2 V, both versus Ag/AgCl (3 M KCl).

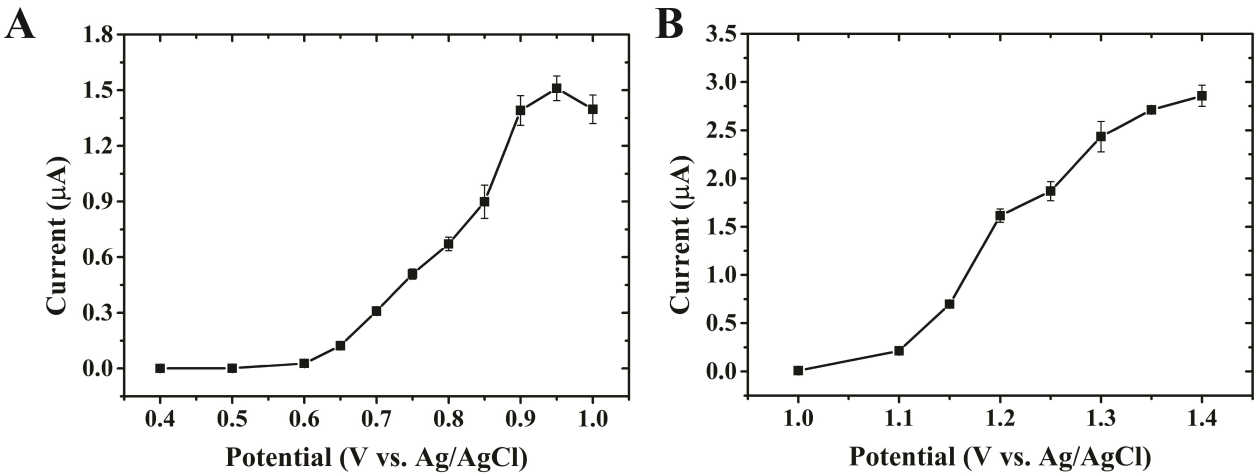

FIGURE 7 | Hydrodynamic voltammograms for (A) 100 μM DCF in 0.1 M PB (pH 7.2) and (B) 100 μM CBZ in 0.1 M $HClO_4$ at a BDD electrode. Flow rate = 1 mL min^{-1}. Injection volume = 20 μL. Data are presented as mean ± std. dev. for three injections at each potential.

Figure 8B presents replicate injections of CBZ in the FIA-EC mode at different analyte concentrations from 100 down to 0.1 μM. The carrier solution was 0.1 M $HClO_4$. Three injections of each concentration were made to assess the response reproducibility. Reproducible current responses are seen for each concentration. Figure 8B inset shows the calibration curve of peak current versus injected concentration of CBZ. The response sensitivity was 8.8 ($\pm$0.4) μA mM^{-1} with good linearity across the concentration range ($r^2 > 0.995$).

The theoretical minimum concentration detectable for DCF and CBZ dissolved in standard solutions was determined to be 23.6 $\pm$ 0.2 and 75.9 $\pm$ 0.3 nM, respectively. This value was calculated by 3 s/m with s being the noise and m being the slope of the response curve. These concentrations for DCF and CBZ are below the lowest concentration studied in this work of 100 nM.

Percentage recoveries of DCF and CBZ in the spiked urine simulant were determined in the FIA-EC mode and values are shown in Table 2. The urine simulant samples were prepared in 1:1 urine simulant:0.1 M PB (pH 7.2) mixture for DCF and 1:1 urine simulant:0.1 M $HClO_4$ mixture for CBZ. The concentration of both drugs was 10 μM. Representative FIA responses for 10 μM concentrations of each drug and corresponding blank injections are presented in Figure S3. The urine simulant contains electrolyte ions different from the carrier solutions (e.g. magnesium, calcium, sulfate, etc.), which generate a non-faradaic current response when injected due to changes in the interfacial electric double layer. There are also electrochemically- active species in the urine simulant (e.g. chloride, urea, creatinine) that can be oxidized at BDD electrodes and producing faradaic current at the more positive potentials [46–48].

The electrolyte solutions were a 1:1 dilution of the urine simulant in either 0.1 M PB (pH 7.2) for DCF or 0.1 M $HClO_4$ for CBZ. The recovery values were determined by dividing the mean value of calculated drug concentration by the true concentration and multiplying by 100.

Compared to the SWV detection data in Table 1, the FIA-EC method afforded better accuracy (closer to 100% recovery) and improved reproducibility for determining the DCF and CBZ concentrations in the spiked urine simulant. For both drugs, the FIA-EC method produced nominal percent recoveries that were statistically similar to the theoretical 10 μM injected. Based on the calibration plot generated using external standards, the theoretical current for a 10 μM injection of DCF is 0.048 μA. At the 95% confidence interval, this current falls within the expected range 0.049 $\pm$ 0.002 μA for measured values. Based on the calibration plot generated using external standards, the theoretical current for a 10 μM injection of CBZ is 0.163 μA. At the 95% confidence interval, this current falls within the expected range of 0.165 $\pm$ 0.008 μA for measured values. The percentages being slightly greater than 100% is attributed to some extra current arising from the oxidation of species in the urine simulant in addition to the drug as the

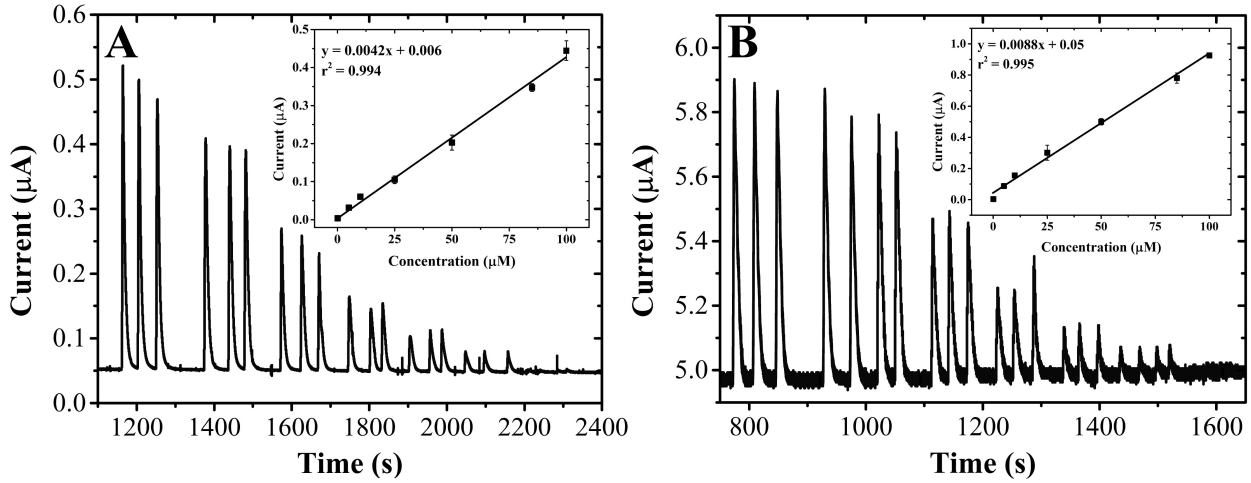

FIGURE 8 | Replicate FIA-EC injections of (A) DCF in 0.1 M PB (pH 7.2) and (B) CBZ in 0.1 M $HClO_4$ at concentrations from 100 to 0.1 μM. The detection potential for DCF was 1.0 V and for CBZ was 1.4 V vs. Ag/AgCl (3 M KCl). Insets show corresponding calibration curves of the nominal peak current versus the concentration for the respective drugs. Data are presented for the mean $\pm$ std. dev. of three injections of each concentration at a single BDD thin-film electrode. Flow rate = 1 mL min^{-1}.

TABLE 2 | FIA-EC oxidation currents for 10 μM DCF and CBZ in spiked urine simulant samples at three different BDD thin-film electrodes.

Pollutant	BDD 1 (μA)	BDD 2 (μA)	BDD 3 (μA)	Mean $\pm$ Std. Dev. (μA)	Calculated (μM)	Recovery (%)
DCF	0.050	0.050	0.048	0.049 $\pm$ 0.001	10.3 $\pm$ 0.2	102
CBZ	0.166	0.167	0.161	0.165 $\pm$ 0.003	10.1 $\pm$ 0.2	101

calibrations curves were generated using 0.1 M PB (pH 7.2) and 0.1 M $HClO_4$, respectively, as the carrier solutions for DCF and CBZ with no urine simulant added.

3.5 | Response Reproducibility and Stability in Flow Injection Analysis

Figure 9 presents the short-term response reproducibility data for thirty 20-μL injections of (A) 100 μM DCF in 0.1 M PB (pH 7.2) and (B) 100 μM CBZ in 0.1 M $HClO_4$ at a BDD electrode. Figure 9 presents the short-term response reproducibility data for thirty 20-μL injections of (A) 100 μM DCF in 0.1 M PB (pH 7.2) and (B) 100 μM CBZ in 0.1 M $HClO_4$ at a BDD electrode. The relative standard deviation of the peak height was 4.90% for DCF and 3.81% for CBZ. The results demonstrate that the BDD electrode provides good short-term response reproducibility for the oxidative detection of these two pharmaceuticals using FIA-EC detection. The interday response stability of the electrodes was then tested over the course of eight consecutive days. The results are presented in Figure 9C and D for DCF and CBZ, respectively. For DCF, the response decreases by 25% on Days 1–3 before stabilizing afterward with an RSD of 5.43% for days 3–8. For CBZ, a stable response is seen over the entire period with an RSD of 2.02%. The response trend for DCF in Figure 9A and C is consistent with the response attenuation seen in the voltammetric measurements and highlights the importance of cleaning the BDD surface with distilled isopropanol periodically between measurements.

Table 3 provides a comparison of detection figures of merit reported for several electrochemical assays for DCF and CBZ. The detection figures of merit reported herein for BDD electrodes are as good or superior to the figures of merit reported in the literature for BDD and other electrodes. In other words, the limit of detection (LOD), linear dynamic range (LDR), and reproducibility reported herein for this BDD-based assay are close to state-of-the-art.

4 | Discussion

In this work, the electrooxidation of DCF and CBZ in standard solutions and a urine simulant were investigated by voltammetric methods and flow injection analysis with amperometric

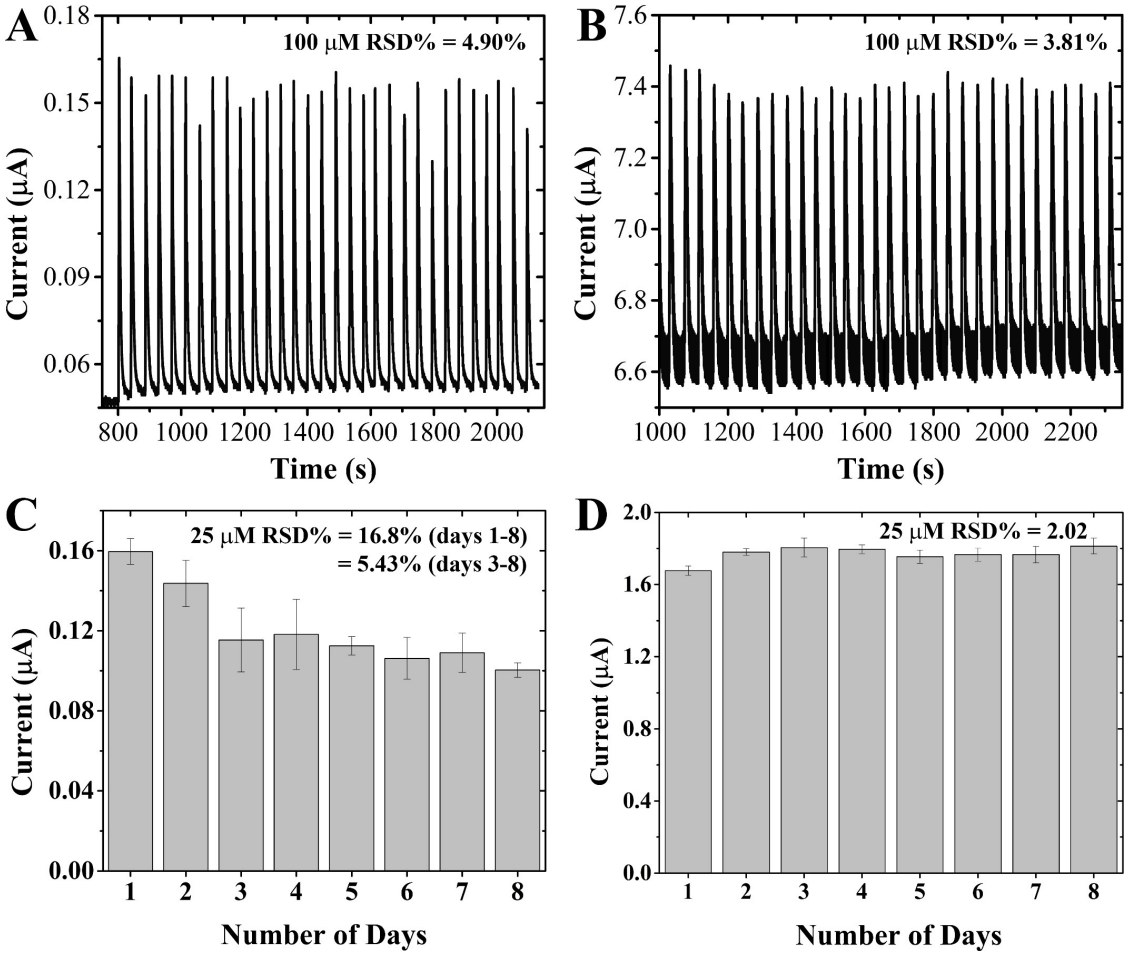

FIGURE 9 | Short-term response reproducibility for 30 injections of (A) 100 μM DCF in 0.1 M PB (pH 7.2) and (B) 100 μM CBZ in 0.1 M $HClO_4$ using a single BDD electrode. The interday response stability of (C) 25 μM DCF in 0.1 M PB (pH 7.2) and (D) 25 μM CBZ in 0.1 M $HClO_4$ over eight consecutive days are presented. Data are presented as mean +/- std. dev. for 30 injections. Flow rate = 1 mL min^{-1}. Injection volume = 20 μL. The detection potential for DCF was 1.0 V and for CBZ was 1.4 V vs. Ag/AgCl (3 M KCl).

TABLE 3 | Comparison of the detection figures of merit for DCF and CBZ using BDD (this work) with other data reported in the literature.

Electrode	Method/ pollutant	LOD (μM)	LDR (μM)	RSD (%)	Reference
CCe/MWCNT	DPV/DCF	0.0027	0.05–20	4	[24]
GCE-Cu/$ZnFe_2O_4$/rGO	DPV/CBZ	0.003	0.01–90	2.83	[30]
ILCNPE	SWV/DCF	0.09	0.3–750	2.40	[23]
BCNW	DPV/CBZ	4.76	1–50	–	[29]
BDD	FIA-MPA/DCF	0.14	5–50	1.00	[33]
Au-rGO-AuNPs	LSV/CBZ	3.03	0.1–100	–	[51]
FULL/CNT	DPV/DCF	0.23	0.34–1.7	0.45	[52]
MoSe2-rGO/SPCE	DPV/CBZ	0.007	0.02–380	4.8	[53]
BDD	FIA-EC/ DCF	0.0236 ± 0.0002	0.1–100	4.90	This work
BDD	FIA-EC/ CBZ	0.0776 ± 0.0003	0.1–100	3.81	This work

Abbreviations: LOD, limit of detection;LDR, linear dynamic range;RSD, relative standard deviation;GCE, glassy carbon electrode;CPE, carbon paste electrode;SPCE, screen printed carbon electrode;Fe/SiO2, iron-doped silicon oxide nanoparticles;Au-Gr-AuNPs, graphene gold nanoparticles composite deposited on gold electrode; NC-fMWCNTs, nanocellulose functionalized multiwalled carbon nanotubes;ILCNPE, ionic liquid carbon nanotube paste electrode;FULL/CNT, fullerene carbon nanofiber;Ce-ZnO/rGO, cerium-doped zinc oxide and reduced graphene oxide;CCE, carbon ceramic electrode;LSV, linear sweep voltammetry;DPV, differential pulse voltammetry

detection using boron-doped nanocrystalline diamond thin-film electrodes. For DCF, two oxidation peaks were observed in the cyclic voltammetric measurements at *ca.* 0.7 and 1.05 V. The 0.7 V peak is attributed to the $2e^-/2H^+$ oxidation to form the dimer as shown in Figure 1. The anodic current at 1.05 V is likely a further oxidation reaction of the dimer product [24]. The DCF oxidation at 0.7 V is diffusion controlled as evidenced by the linearity of the i_p^{ox} vs scan rate$^{1/2}$ plot. This was not a straightforward measurement as the electrode surface had to be cleaned between each scan by immersion in ultrapure isopropanol to remove adsorbed DCF and or oxidation reaction products. As noted in the *Results* section, a reversible redox couple appeared centered at 0.3 V after the first positive-going, oxidative scan out to 1.2 V. This was followed by a 20% diminution in the DCF peak current at 0.7 V in subsequent scans even after mixing the solution to eliminate the depletion layer at the electrode surface. The adsorption of the reversible redox couple was confirmed using an immersion experiment in which, after several potential cycles, the 100 μM DCF working solution was replaced with drug-free 0.1 M PB (pH 7.2) electrolyte and the cyclic voltammetric scans were then repeated. The reversible couple at 0.3 V was still present in the neat buffer with the irreversible peaks at 0.7 and 1.05 V disappearing. A 5-min soak of the electrode in ultrapure isopropanol eliminated the redox couple at 0.3 V by dissolving it off the surface. We suspect the accumulation of adsorbed redox species (*i.e.*, electrode fouling) is partially responsible for the attenuated DCF oxidation peak current at 0.7 V during repeat voltammetric scans. This fouling reduces the electroactive area available for subsequent DCF molecule oxidation.

We did not perform experiments specifically to try and identify the redox couple or determine its surface coverage. Observationally though, the largest peak currents for the reversible couple at 0.3 V were observed after the first cycle in neat 0.1 M PB (pH 7.2) solution. The peak currents decreased and the ΔE_p increased with cycle number. It is uncommon to find redox reactions that proceed through an adsorbed state on BDD electrodes as molecular interactions with the surface tend to be weak. The adsorption of the redox couple was observed on electrodes that were initially pretreated in a hydrogen plasma. This produces a low oxygen surface (*e.g.*, ~ XPS O/C atomic ratio of 0.02) with few surface carbon-oxygen functional groups. A pseudo-positively charged surface therefore exists with the more electropositive hydrogen surface layer ((δ+)H–C(δ−)). This means weak dipole-dipole and ion-dipole surface interactions with the redox analyte are possible and may be a mechanism by which the reaction product(s) interacts with the surface. The Raman spectra in Figure S1 exhibit a weakly intense peak at 1545 cm^{-1} reflective of some low levels of non-diamond sp^2 carbon impurity. Therefore, the DCF oxidized product(s) may adsorb on the electrode through π–π interactions with the sp^2 impurity sites. These two adsorption mechanisms may be responsible for the cycle dependent electrochemical response of DCF at the BDD electrodes.

The oxidatively generated redox couple observed at 0.3 V in Figure 2 has demonstrated pH-dependence in the published literature [22]. Based on the redox potential and proton-transfer mechanism, this species could be a hydroquinone/quinone redox couple. It is possible that the electrochemically formed DCF dimers (Figure 1) first react with water to form a hydroxyl group on the substituted phenylacetic acid ring. Subsequent hydrolysis of the amine bond could form a hydroquinone species that would be electrochemically active at 0.3 V in pH 7.2 buffer. Several authors have noted the DCF oxidation is accompanied by an increase in solution absorbance at 450 nm from the extended aromatic conjugation in the DCF dimers [22, 54]. Over time in aqueous solution, the 450 nm peak absorbance decreases as the oxidized products are hydrolyzed.

The loss of conjugation after hydrolysis to form a hydroquinone would both explain the decrease in absorbance at 450 nm and the redox feature at 0.3 V.

Gimenes and coworkers have similarly used heavily doped BDD thin-film electrodes to detect DCF using FIA [33]. The present work improves upon this report in several ways. We achieved a *ca.* 6-times lower theoretical detection limit towards DCF (0.0236 vs. 0.14 μM) and applied lower detection potentials (1 vs 1.2 V). The DCF oxidation was shifted to lower detection potentials by using pH 7.2 electrolyte. This change improved the signal-to-noise (S/N) ratio and lowered the detection limit. Further, we used slower flow rates (1 vs. 3 mL min^{-1}), and injected smaller sample volumes (20 vs. 50 μL). This decreases both the solvent waste and amount of sample required for analysis. Notably, Gimenes et al. achieved greater sensitivity than achieved in this work (4.2 vs 89.9 μA mM^{-1}). The authors utilized multiple pulse amperometry (MPA), which offers better sensitivity than continuous amperometry used in the present work. Despite their higher sensitivity, Gimenes et al. report a higher detection limit than achieved in this report due to their low S/N ratio. An improved method could combine MPA detection (as done by Gimenes et al.), a neutral pH electrolyte, and slow flow rates (as in this work) to improve both the sensitivity and S/N ratio.

The CBZ oxidation is observed at 1.2 V in 0.1 M $HClO_4$ at BDD thin-film electrodes. This current is attributed to the proposed CBZ redox reaction shown in Figure 1. The CBZ oxidation current was twice the magnitude of DCF. CBZ oxidation involves a four-electron transfer whereas DCF only involves a two-electron transfer–so this result is expected. Over successive CV cycles at 100 μM CBZ, the oxidation peak current decreased. We also attribute this behavior to the formation of a depletion layer since the oxidation reaction does not generate reducible products and mixing restores the current. Mixing the solution with a Pasteur pipette eliminated the formed depletion layer, and the current was fully restored. When the CV was performed with 1 mM CBZ (Figure S4) reversible two-step redox current appeared at 0.4 V after the direct CBZ oxidation at 1.2 V. Since this species was dependent on CBZ oxidation, it is likely a CBZ intermediate or product. The CBZ solution was emptied from the cell, the cell gently rinsed with DI water, and then 0.1 M $HClO_4$ electrolyte added. A subsequent CV revealed the reversible species was still present at 0.4 V, but the CBZ oxidation at 1.2 V disappeared. Further, the redox current at 0.4 V disappeared after a short 5-min soak in ultrapure IPA. This shows the species producing the current was surface absorbed. The reversible compound only appeared at higher concentrations. It is likely present in small amounts at 100 μM, but not enough to hinder CBZ detection.

The CBZ oxidation reaction occurs at more positive potentials. Therefore, with repeated scans to the positive potentials for detection, carbon-oxygen functional groups are expected to be introduced at the non-diamond sp^2 carbon impurity on the BDD surface. This would create a pseudo-negatively charged surface with the more electronegative oxygen surface layer ($(\delta-)O-C(\delta+)$). At pH 1, CBZ and possible products would have a positive formal charge due to protonation of the terminal carbamide nitrogen. A cationic species could adsorb to the surface through dipole-dipole interactions. Likely, the positively charged products would be highly solvated by water molecules which competes with the dipole-dipole forces between the product and the surface. Since they are highly solvated by water, the products only weakly interact with the surface and there is minor change in the electrochemically active surface area, especially at low CBZ concentrations. The product therefore has little influence on the CBZ detection in the concentration range examined for the SWV and FIA studies.

We decided to measure DCF oxidation in neutral PB for two reasons. Firstly, it is a more biologically relevant pH (e.g. blood, urine) that is easily buffered. Secondly, the DCF oxidation potential is more negative at neutral pH. This offers better selectivity since many species are electrochemically active at $\geq$0.8 V. We initially measured CBZ in 0.1 M PB (pH 7.2). There were a few challenges to measuring the drug in this electrolyte. Namely, the background current was larger at pH 7.2 compared to pH 1 because of the increased oxygen evolution current at neutral pH. We also observed the CBZ oxidation peak current is about 2-fold larger in $HClO_4$ (pH 1) compared to PB (pH 7.2). This decreased CBZ current at neutral pH has been observed on modified carbon electrodes [31]. The combination of lower background and larger signal make the measurement of CBZ in 0.1 M $HClO_4$ more sensitive and reproducible. Since DCF and CBZ have poor solubility $\geq$1 mM, both drugs were dissolved in methanol to create 10 mM stock solutions. Working solutions were prepared from this stock and completed to 1% (v/v) methanol to have consistent organic fraction across experiments.

The detection potentials for DCF and CBZ were consistent at varied scan rates (CV, Figure 3) and varied concentrations (SWV, Figure 4). Therefore, we applied 1.0 and 1.4 V for FIA detection of DCF and CBZ, respectively. In the FIA studies the DCF current is about 10-fold lower than SWV. This is attributed to the smaller electrode area in the flow cell (flow cell for FIA = *ca.* 0.10 cm^{-1}, glass cell for SWV = *ca.* 0.32 cm^{-1}) and electrode fouling after successive FIA measurements. During the SWV studies, the electrode was soaked with IPA for at least 5 min between each measurement to remove adsorbed products. This maintained the same electrochemically active surface area for successive DCF concentrations which resulted in higher currents. However, the FIA was done in a continuous flow without IPA cleaning steps between injections. The electrode becomes coated with oxidized DCF products, which reduces the exposed electroactive area and decreases the current. Since the FIA calibration of DCF is highly reproducible, the surface coverage of fouling products reaches a constant value but does not completely block the surface. Despite this coverage, the measurement is still very sensitive due to the low background current at the applied potential.

The FIA background current is much larger for CBZ as compared to DCF. This occurs because the CBZ oxidation requires a larger applied potential, which increases the background current and noise. Even so, the CBZ current is double that of DCF because it is a four-electron transfer oxidation. This generates a larger signal that improves the signal-to-noise ratio. With the parameters used, the CBZ detection by FIA is

very sensitive, despite the noisy background. Zhang and coworkers have noted how the voltammetric response of authentic urine specimens at BDD electrodes can be complex, especially at the detection potentials used in this work [55]. The FIA-EC studies presented herein serve as proof-of-concept to establish (i) the parameters required for sensitive detection of DCF and CBZ at BDD electrodes and (ii) that their detection can be performed in a more complex biological matrix in addition to a standard solution. An additional analytical method, like liquid chromatography, would be required to impart selectivity to this electrochemical detection strategy to avoid electroactive interferents at the chosen detection potential in more complex matrices. Compared to other electrochemical detection strategies, detecting CBZ and DCF by FIA at thin-film BDD nanocrystalline electrodes achieves impressive nanomolar detection limits. Further, the BDD electrodes do not require complex, multi-step electrode modifications which makes for a highly reproducible method with very stable interday electrode performance.

5 | Conclusions

The electrochemical detection of two pharmaceuticals, dichlofenac and carbamazepine, in standard solutions and a urine simulant were demonstrated by voltammetric methods and flow injection analysis with amperometric detection using boron-doped nanocrystalline diamond thin-film electrodes. For DCF, two primary oxidation peaks were observed in the cyclic voltammetric measurements at *ca.* 0.7 and 1.05 V vs. Ag/AgCl. For CBZ, one primary oxidation peak was seen at ca. 1.2 V vs. Ag/AgCl. The primary oxidation peak currents for both drugs were limited by diffusion, however, the DCF oxidation produced a product that adsorbed on the electrode and contributed to electrode fouling. In square wave voltammetry, the linear dynamic range for both drugs was from at least 0.1 to 100 μM. The nominal sensitivity for DCF in 0.1 M PB (pH 7.2) was $57.3 \pm 2.5\ \mu A\ mM^{-1}$ and for CBZ in 0.1 M $HClO_4$ was $162.3 \pm 4.3\ \mu A\ mM^{-1}$. The higher sensitivity for CBZ is due to more electrons transferred per molecule in the redox reaction. In flow injection analysis with amperometric detection, the linear dynamic range for both drugs was at least from 0.1 to 100 μM. The theoretical detection limits were calculated to be 24 nM and 76 nM, respectively, for DCF and CBZ. The short-term response reproducibility was 4.90% for DCF and 3.81% for CBZ. Excellent response stability was observed for CBZ over eight days of use. After a 25% response loss for DCF between Days 1 and 3, good response stability was seen on Days 3–8. The percent recoveries for both drugs in a urine simulant were 100%. In summary, BDD electrodes provide excellent detection figures of merit for these two drugs in both standard solutions and a urine simulant.

Acknowledgments

The research was supported, in part, from the Army Research Office (GMS) through grant #W911-NF-14-10063. SZ acknowledges the Fulbright Scholar Program through the National Research Foundation (145308) in South Africa and the Institute for Nanotechnology and Water Sustainability at the University of South Africa for financial support. The research was also supported by the National Science Foundation under Grant No. CHE-2150173 (MS and GMS). Any opinions, findings, and conclusions or recommendations expressed in this material are those of the author(s) and do not necessarily reflect the views of the National Science Foundation.

Conflicts of Interest

The authors declare no conflicts of interest.

Data Availability Statement

Most of the raw and treated data obtained are presented in this manuscript. Data will be shared upon appropriate request.

References

1. K. Samal, S. Mahapatra, M. H. Ali, "Pharmaceutical wastewater as Emerging Contaminants (EC): Treatment technologies, impact on environment and human health", *Energy Nexus.* 6 (2022): 100076, https://doi.org/10.1016/j.nexus.2022.100076.

2. J. Sharma, M. Joshi, A. Bhatnagar, A. K. Chaurasia, S. Nigam, "Pharmaceutical residues: One of the significant problems in achieving 'clean water for all' and its solution", *Environmental Research* 215, no. 1 (2022): 114219. https://doi.org/10.1016/j.envres.2022.114219.

3. M. de Oliveira, B. E. F. Frihling, J. Velasques, F. J. C. M. Filho, P. S. Cavalheri, L. Migliolo, "Pharmaceuticals residues and xenobiotics contaminants: Occurrence, analytical techniques and sustainable alternatives for wastewater treatment", *Science of the Total Environment* 705 (2020): 135568, https://doi.org/10.1016/j.scitotenv.2019.135568.

4. C. Gadipelly, A. Pérez-González, G. D. Yadav, I. Ortiz, R. Ibáñez, V. K. Rathod, K. V. Marathe, "Pharmaceutical Industry Wastewater: Review of the Technologies for Water Treatment and Reuse", *Industrial and Engineering Chemistry Research* 53, no. 29 (2014): 11571–11592, https://doi.org/10.1021/ie501210j.

5. Q. Sui, D. Wang, W. T. Zhao, J. Huang, G. Yu, X. Q. Cao, Z. F. Qiu, S. G. Lu, "Pharmaceuticals and consumer products in four wastewater treatment plants in urban and suburb areas of Shanghai", *Environmental Science and Pollution Research* 22, no. 8 (2015): 6086–6094, https://doi.org/10.1007/s11356-014-3793-8.

6. T. aus der Beek, F. A. Weber, A. Bergmann, S. Hickmann, I. Ebert, A. Hein, A. Küster, "Pharmaceuticals in the environment-global occurrences and perspectives", *Environmental Toxicology and Chemistry* 35, no. 4 (2016): 823–835, https://doi.org/10.1002/etc.3339.

7. T. A. Ternes, M. Meisenheimer, D. McDowell, F. Sacher, H. J. Brauch, B. H. Gulde, G. Preuss, U. Wilme, N. Z. Seibert, "Removal of Pharmaceuticals during Drinking Water Treatment", *Environmental Science and Technology* 36, no. 17 (2002): 3855–3863, https://doi.org/10.1021/es015757k.

8. N. M. Vieno, H. Härkki, T. Tuhkanen, L. Kronberg, "Occurrence of pharmaceuticals in river water and their elimination a pilot-scale drinking water treatment plant", *Environmental Science and Technology* 41, no. 14 (2007): 5077–5084, https://doi.org/10.1021/es062720x.

9. P. H. Roberts, K. V. Thomas, "The occurrence of selected pharmaceuticals in wastewater effluent and surface waters of the lower Tyne catchment", *Science of the Total Environment* 356, no. 1–3 (2006): 143–153, https://doi.org/10.1016/j.scitotenv.2005.04.031.

10. M. Gros, M. Petrović, A. Ginebreda, D. Barceló, "Removal of pharmaceuticals during wastewater treatment and environmental risk assessment using hazard indexes", *Environment International* 36, no. 1 (2010): 15–26, https://doi.org/10.1016/j.envint.2009.09.002.

11. R. C. Pivetta, C. Rodrigues-Silva, A. R. Ribeiro, S. Rath, "Tracking the occurrence of psychotropic pharmaceuticals in Brazilian wastewater treatment plants and surface water, with assessment of environmental risks", *Science of the Total Environment* 727 (2020): 138661, https://doi.org/10.1016/j.scitotenv.2020.138661.

12. J. S. Gamarra Jr., A. F. L. Godoi, E. C. de Vasconcelos, K. M. T. de Souza, C. M. R. de Oliveira, "Environmental Risk Assessment (ERA) of diclofenac and ibuprofen: A public health perspective," *Chemosphere* 120 (2015): 462–469. https://doi.org/10.1016/j.chemosphere.2014.08.020

13. W. Boumya, N. Taoufik, M. Achak, H. Bessbousse, A. Elhalil, N. Barka, "Electrochemical sensors and biosensors for the determination of diclofenac in pharmaceutical, biological and water samples", *Talanta Open* 3 (2021) 100026, https://doi.org/10.1016/j.talo.2020.100026.

14. P. McGettigan, D. Henry, "Use of Non-Steroidal Anti-Inflammatory Drugs that Elevate Cardiovascular Risk: An Examination of Sales and Essential Medicines Lists in Low-, Middle-, and High-Income Countries", *PLoS Medicine* 10, no. 2 (2013): e1001388, https://doi.org/10.1371/journal.pmed.1001388.

15. D. Ceron-Litvoc, B. G. Soares, J. Geddes, J. Litvoc, M. S. de Lima, "Comparison of carbamazepine and lithium in treatment of bipolar disorder: A systematic review of randomized controlled trials," *Human Psychopharmacology* 24, no. 1 (2009): 19–28. https://doi.org/10.1002/hup.990

16. J. Winkelmann, R. P. Allen, B. Högl, Y. Inoue, W. Oertel, A. V. Salminen, J. W. Winkelman, C. Trenkwalder, C. Sampaio, "Treatment of restless legs syndrome: Evidence-based review and implications for clinical practice (Revised 2017)", *Movements Disorders* 33, no. 7 (2018): 1077–1091, https://doi.org/10.1002/mds.27260.

17. S. Latifi, T. Messer, "The Efficacy of Tiapride and Carbamazepine Combination Therapy in Reducing Alcohol Withdrawal Symptoms: A Systematic Review and Meta-Analysis", *Pharmacopsychiatry* 52, no. 5 (2019): 209–216, https://doi.org/10.1055/a-0795-3689.

18. C. Y. Ojemaye, L. Petrik, "Occurrences, levels and risk assessment studies of emerging pollutants (pharmaceuticals, perfluoroalkyl and endocrine disrupting compounds) in fish samples from Kalk Bay harbour, South Africa", *Environmental Pollution* 252 (2019): 562–572, https://doi.org/10.1016/j.envpol.2019.05.091.

19. A. Mirzaei, Z. Chen, F. Haghighat, L. Yerushalmi, "Removal of pharmaceuticals and endocrine disrupting compounds from water by zinc oxide-based photocatalytic degradation: A review", *Sustainable Cities and Society* 27 (2016): 407–418, https://doi.org/10.1016/j.scs.2016.08.004.

20. Y. Zhang, S.-U. Geißen, C. Gal, "Carbamazepine and diclofenac: Removal in wastewater treatment plants and occurrence in water bodies", *Chemosphere* 73, no. 8 (2008): 1151–1161, https://doi.org/10.1016/j.chemosphere.2008.07.086.

21. R. R. Singh, A. Lai, J. Krier, T. Kondić, P. Diderich, E. L. Schymanski, "Occurrence and Distribution of Pharmaceuticals and Their Transformation Products in Luxembourgish Surface Waters", *ACS Environmental Au* 1, no. 1 (2021): 58–70, https://doi.org/10.1021/acsenvironau.1c00008.

22. F. W. D. S. Lucas, L. H. Mascaro, T. P. Fill, E. Rodrigues-Filho, E. Franco-Junior, P. Homem-de-Mello, P. de Lima-Neto, A. N. Correia, "Diclofenac on Boron-Doped Diamond Electrode: From Electroanalytical Determination to Prediction of the Electrooxidation Mechanism with HPLC-ESI/HRMS and Computational Simulations", *Langmuir* 30, no. 19 (2014): 5645–5654, https://doi.org/10.1021/la4044123.

23. M. Goodarzian, M. A. Khalilzade, F. Karimi, V. K. Gupta, M. Keyvanfard, H. Bagheri, M. Fouladgar, "Square wave voltammetric determination of diclofenac in liquid phase using a novel ionic liquid multiwall carbon nanotubes paste electrode", *Journal of Molecular Liquids* 197 (2014): 114–119, https://doi.org/10.1016/j.molliq.2014.04.037.

24. H. Razmi, K. Sarhang-Zadeh, R. Mohammad-Rezaei, "Electrochemical Behavior and Voltammetric Determination of Diclofenac at a Multi-Walled Carbon Nanotube-Ionic Liquid Composite Modified Carbon Ceramic Electrode", *Analytical Letters* 46, no. 12 (2013): 1885–1896, https://doi.org/10.1080/00032719.2013.777919.

25. Ľ. Švorc, J. Sochr, P. Tomčík, M. Rievaj, D. Bustin, "Simultaneous determination of paracetamol and penicillin V by square-wave voltammetry at a bare boron-doped diamond electrode", *Electrochimica Acta* 68 (2012): 227–234, https://doi.org/10.1016/j.electacta.2012.02.071.

26. M. Ferreira, S. Güney, I. Kuźniarska-Biernack, O. S. G. P. Soares, J. L. Figueiredo, M. F. R. Pereira, I. C. Neves, A. M. Fonseca, P. Parpot, "Electrochemical oxidation of diclofenac on CNT and M/CNT modified electrodes", *New Journal of Chemistry* 45, no. 28 (2021): 12622–12633, https://doi.org/10.1039/D1NJ01117K.

27. A. C. Lazanas, M. I. Prodomidis, "Large surface vanadium pentoxide nanosheet modified screen-printed electrode for nanomolar diclofenac determination", *Electrochimica Acta* 428 (2022): 140919, https://doi.org/10.1016/j.electacta.2022.140919.

28. J. G. Teixeira, A. Veiga, A. J. P. Carvalho, D. M. Teixeira, "Electrooxidation of carbamazepine metabolites: Characterization and influence in the voltammetric determination of the parent drug", *Electrochimica Acta* 108 (2013): 51–65, https://doi.org/10.1016/j.electacta.2013.06.070.

29. M. Pierpaoli, A. Dettlaff, M. Szopińska, K. Karpienko, M. Wróbel, A. Łuczkiewicz, S. Fudala-Książek, R. Bogdanowicz, "Simultaneous opto-electrochemical monitoring of carbamazepine and its electrooxidation by-products in wastewater", *Journal of Hazardous Materials* 419 (2021): 126509, https://doi.org/10.1016/j.jhazmat.2021.126509.

30. M. Ghalkhani, E. M. Khosrowshahi, E. Sohouli, K. Eskandari, M. Aghaei, M. Rahimi-Nasrabadi, A. Sobhani-Nasab, H. Banafshe, E. Kouchaki, "Electrochemical monitoring of carbamazepine in biological fluids by a glassy carbon electrode modified with CuO/ZnFeO/rGO nanocomposite", *Surfaces and Interfaces* 30(2022): 101943, https://doi.org/10.1016/j.surfin.2022.101943.

31. N. Qambrani, J. A. Buledi, N. H. Khand, A. R. Solangi, S. Ameen, N. S. Jalbani, A. Khatoon, M. A. Taher, F. H. Moghadam, M. Shojaei, F. Karimi, "Facile Synthesis of NiO/ZnO nanocomposite as an effective platform for electrochemical determination of carbamazepine", *Chemosphere* 303 (2022): 135270, https://doi.org/10.1016/j.chemosphere.2022.135270.

32. M. Ihos, A. Remes, F. Manea, "Electrochemical Determination of Diclofenac Using Boron-Doped Diamond Electrode," *Journal of Environmental Protection and Ecology* 13, no. 4 (2012): 2096–2103.

33. D. T. Gimenes, J. M. de Freitas, R. A. A. Munoz, E. M. Richter, "Flow-Injection Amperometric Method for Determination of Diclofenac in Pharmaceutical Formulations Using a Boron-Doped Diamond Electrode", *Electroanalysis* 23, no. 11 (2011): 2521–2525, https://doi.org/10.1002/elan.201100126.

34. S. Feijoo, M. Kamali, Q.-K. Pham, A. Assoumani, F. Lestremau, D. Cabooter, R. Dewil, "Electrochemical Advanced Oxidation of Carbamazepine: Mechanism and optimal operating conditions", *Chemical Engineering Journal* 446, no. 3 (2022): 137114, https://doi.org/10.1016/j.cej.2022.137114.

35. A. M. Idris, "An Overview of the Generations and Recent Versions of Flow Injection Techniques", *Critical Reviews in Analytical Chemistry* 40, no. 3 (2010): 150–158, https://doi.org/10.1080/10408340903103437.

36. M. C. Granger, M. Witek, J. Xu, J. Wang, M. Hupert, A. Hanks, M. D. Koppang, J. E. Butler, G. Lucazeau, M. Mermoux, J. W. Strojek, G. M. Swain, "Standard electrochemical behavior of high-quality, boron-doped polycrystalline diamond thin-film electrodes", *Analytical Chemistry* 72, no. 16 (2000): 3793–3804, https://doi.org/10.1021/ac0000675.

37. R. Jarosová, K. Irikura, R. C. Rocha-Filho, G. M. Swain, "Detection of Pyocyanin with a Boron-doped Diamond Electrode Using Flow Injection Analysis with Amperometric Detection and Square Wave Voltammetry," *Electroanalysis* 34, no. 12 (2022): 1902–1912. https://doi.org/10.1002/elan.202100562

38. A. M. Santos, F. C. Vicentini, L. C. S. Figueiredo-Filho, P. B. Deroco, O. Fatibello-Filho, "Flow injection simultaneous determination of

acetaminophen and tramadol in pharmaceutical and biological samples using multiple pulse amperometric detection with a boron-doped diamond electrode", *Diamond and Related Materials* 60 (2015): 1–8, https://doi.org/10.1016/j.diamond.2015.10.005.

39. A. E. Fischer, Y. Show, G. M. Swain, "Electrochemical performance of diamond thin-film electrodes from different commercial sources", *Analytical Chemistry* 76, no. 9 (2004): 2553–2560, https://doi.org/10.1021/ac035214o.

40. S. Alehashem, F. Chambers, J. W. Strojek, G. M. Swain, R. Ramesham, "Cyclic Voltammetric Studies of Charge-Transfer Reactions at Highly Boron-Doped Polycrystalline Diamond Thin-Film Electrodes", *Analytical Chemistry* 67, no. 17 (1995): 2812–2821, https://doi.org/10.1021/ac00113a014.

41. J. Stotter, J. Zak, Z. Behier, Y. Show, G. M. Swain, "Optical and electrochemical properties of optically transparent, boron-doped diamond thin film deposited on quartz", *Analytical Chemistry* 74, no. 23 (2002): 5924–5930, https://doi.org/10.1021/ac0203544.

42. M. C. Granger, G. M. Swain, "The Influence of Surface Interactions on the Reversibility of Ferri/Ferrocyanide at Boron-Doped Diamond Thin-Film Electrodes", *Journal of the Electrochemical Society* 146, no. 12 (1999): 4551, https://doi.org/10.1149/1.1392673.

43. S. Ranganathan, T.-C. Kuo, R. L. McCreery, "Facile preparation of active glassy carbon electrodes with activated carbon and organic solvents", *Analytical Chemistry* 71, no. 16 (1999): 3574–3580, https://doi.org/10.1021/ac981386n.

44. D. Hamblin, J. Qiu, L. Haubold, G. M. Swain, "The performance of a nitrogen-containing tetrahedral amorphous carbon electrode in flow injection analysis with amperometric detection", *Analytical Methods* 7, no. 11 (2015): 4481–4485, https://doi.org/10.1039/C5AY01017A.

45. R. Jarosová, J. Rutherford, G. M. Swain, "Evaluation of a nitrogen-incorporated tetrahedral amorphous carbon thin film for the detection of tryptophan and tyrosine using flow injection analysis with amperometric detection," *The Analyst* 141, no. 21 (2016): 6031–6041. https://doi.org/10.1039/C6AN01379A

46. S. Ferro, A. De Battisti, I. Duo, C. Comninellis, W. Haenni, A. Perret, "Chlorine evolution at highly boron-doped diamond electrodes", *Journal of the Electrochemical Society* 147, no. 7 (2000): 2614–2619, https://doi.org/10.1149/1.1393578.

47. M. Cataldo Hernández, N. Russo, M. Panizza, P. Spinelli, D. Fino, "Electrochemical oxidation of urea in aqueous solutions using a boron-doped thin-film diamond electrode", *Diamond and Related Materials* 44 (2014) 109–116, https://doi.org/10.1016/j.diamond.2014.02.006.

48. Z. Zhang, J. Xian, C. Zhang, D. Fu, "Degradation of creatinine using boron-doped diamond electrode: Statistical modeling and degradation mechanism", *Chemosphere* 182 (2017): 441–449, https://doi.org/10.1016/j.chemosphere.2017.05.057.

49. B. C. Lourencao, T. A. Silva, O. Fatibello-Filho, G. M. Swain, "Voltammetric Studies of Propranolol and Hydrochlorothiazide Oxidation in Standard and Synthetic Biological Fluids Using a Nitrogen-Containing Tetrahedral Amorphous Carbon (ta-C:N) Electrode", *Electrochimica Acta* 143 (2014): 398–406, https://doi.org/10.1016/j.electacta.2014.08.008.

50. R. Jarosová, S. Sanchez, L. Haubold, G. M. Swain, "Isatin Analysis Using Flow Injection Analysis with Amperometric Detection - Comparison of Tetrahedral Amorphous Carbon and Diamond Electrode Performance", *Electroanalysis* 29, no. 9 (2017); 2147–2154.

51. S. Pruneanu, F. Pogacean, A. R. Biris, S. Ardelean, V. Canpean, G. Blanita, E. Dervishi, A. S. Biris, "Novel Graphene-Gold Nanoparticle Modified Electrodes for the High Sensitivity Electrochemical Spectroscopy Detection and Analysis of Carbamazepine", *Journal of Physical Chemistry C* 115, no. 47 (2011): 23387–23394, https://doi.org/10.1021/jp206945e.

52. S. Motoc, F. Manea, A. Baciu, S. Vasilie, A. Pop, "Highly sensitive and simultaneous electrochemical determinations of non-steroidal anti-inflammatory drugs in water using nanostructured carbon-based paste electrodes", *Science of the Total Environment* 846 (2022): 157412, https://doi.org/10.1016/j.scitotenv.2022.157412.

53. M. Hasanpour, A. Pardakhty, S. Tajik, "The development of disposable electrochemical sensor based on MoSe2-rGO nanocomposite modified screen printed carbon electrode for amitriptyline determination in the presence of carbamazepine, application in biological and water samples", *Chemosphere* 308 (2022): 136336, https://doi.org/10.1016/j.chemosphere.2022.136336.

54. M. M. Cid-Cerón, D. S. Guzmán-Hernández, M. T. Ramírez-Silva, A. Galano, M. Romero-Romo, M. Palomar-Pardavé, "New Insigths on the Kinetics And Mechanism of the Electrochemical Oxidation of Diclofenac in Neutral Aqueous Medium", *Electrochimica Acta* 199 (2016): 92–98, https://doi.org/10.1016/j.electacta.2016.03.094.

55. Z. P. Zhang, G. Ogata, K. Asai, T. Yamamoto, Y. Einaga, "Electrochemical Diagnosis of Urinary Tract Infection Using Boron-Doped Diamond Electrodes", *ACS Sensors* 8, no. 11 (2023): 4245–4252, https://doi.org/10.1021/acssensors.3c01569.

Supporting Information

Additional supporting information can be found online in the Supporting Information section at the end of this article.